

## Supporting Information

### A railway-like network electrode design for room temperature Na-S battery

Tingting Yang,<sup>a</sup> Wei Gao,<sup>a</sup> Bingshu Guo,<sup>a</sup> Renming Zhan,<sup>a</sup> Qiuju Xu,<sup>a</sup> Hong He,<sup>a</sup> Shujuan Bao,<sup>a</sup> Xiaoyan Li,<sup>b</sup> Yuming Chen,<sup>\*c</sup> and Maowen Xu<sup>\*a</sup>

<sup>a</sup>Institute for Clean Energy & Advanced Materials, Faculty of Materials and Energy, Southwest University, Chongqing 400715, PR China.

<sup>b</sup>Department of Applied Physics and Institute of Textiles and Clothing, The Hong Kong Polytechnic University, Hong Kong, China.

<sup>c</sup>Department of Nuclear Science and Engineering, Department of Materials Science and Engineering, Massachusetts Institute of Technology, Cambridge, Massachusetts 02139, USA.

\*Corresponding author:

E-mail: xumaowen@swu.edu.cn; yumingc@mit.edu.

## Supplementary Figures

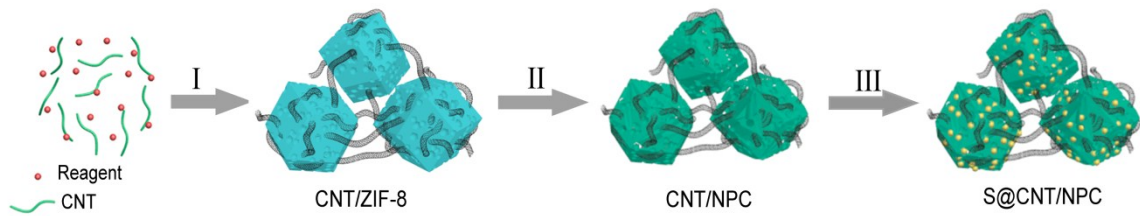


**Fig. S1.** Formation mechanism of S@CNT/NPC composite.

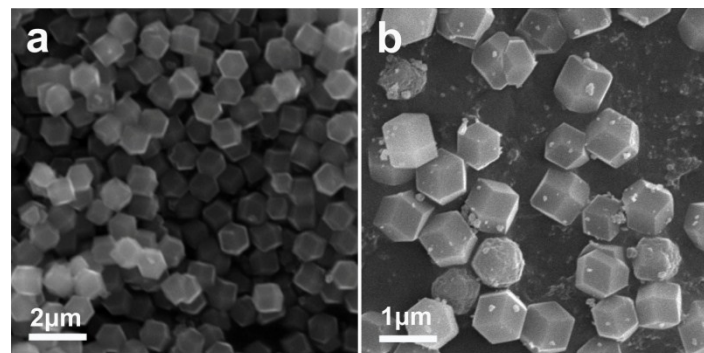


**Fig. S2.** FESEM images of ZIF-8 (a) and NPC (b).

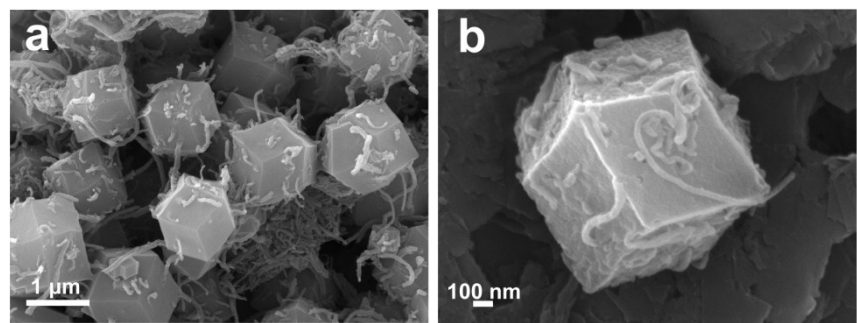


**Fig. S3.** FESEM images (a-b) of CNT/ZIF-8.

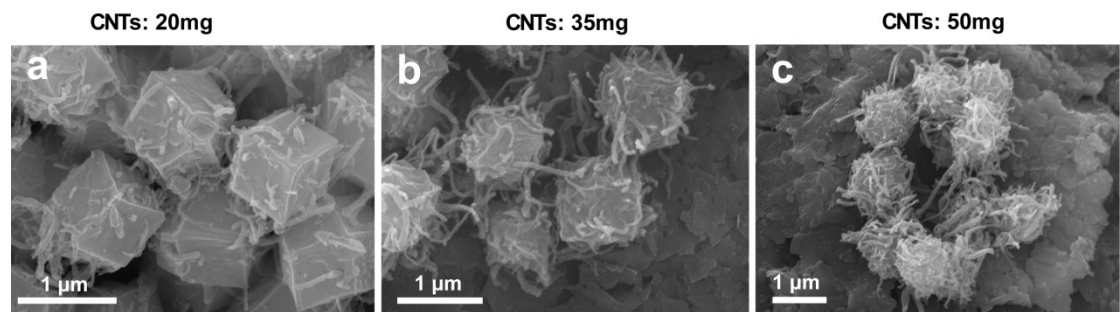


**Fig. S4.** FESEM images (a-c) of CNT/ZIF-8 with different content of CNTs.

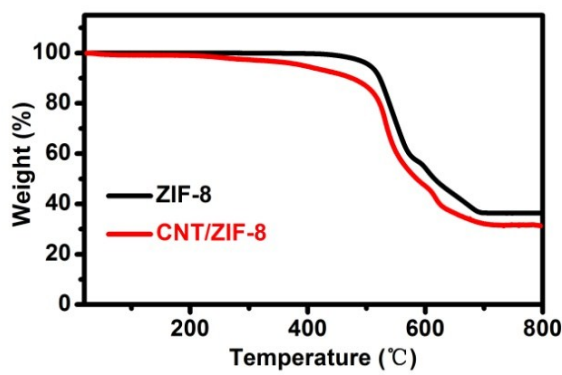


**Fig. S5.** Thermogravimetric analysis (TGA) under oxygen atmosphere.

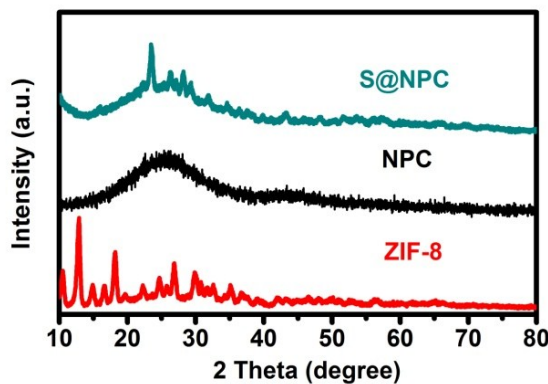


**Fig. S6.** XRD patterns of the ZIF-8, NPC and S@NPC composite.

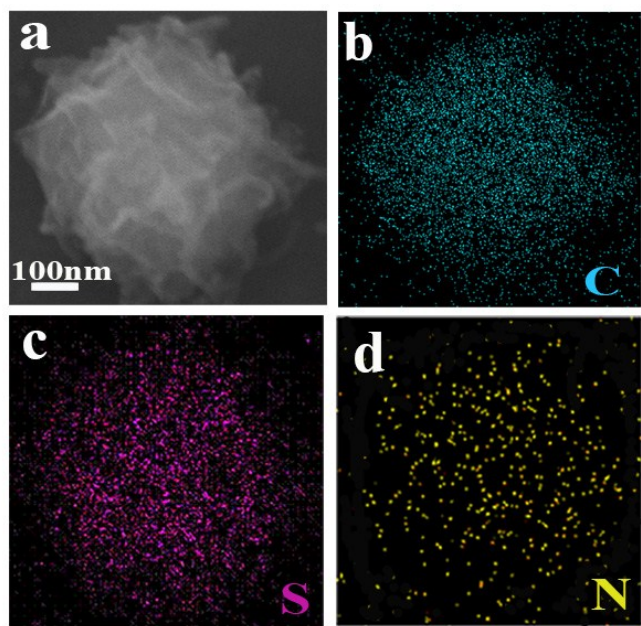


**Fig. S7.** FESEM elemental mapping images of C (b), S (c), and N (d) of S@CNT/NPC composite.

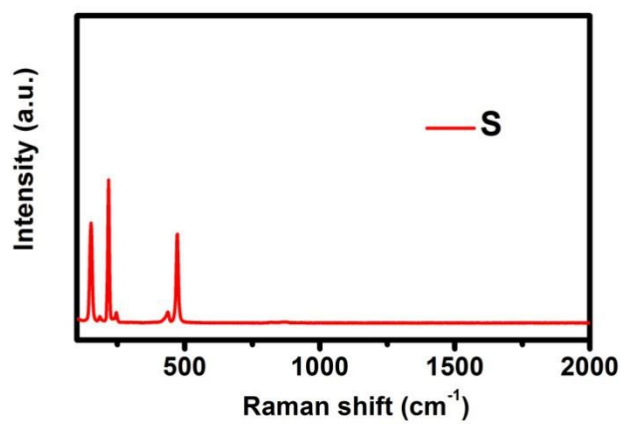


**Fig. S8.** Raman spectrum patterns of pure S.

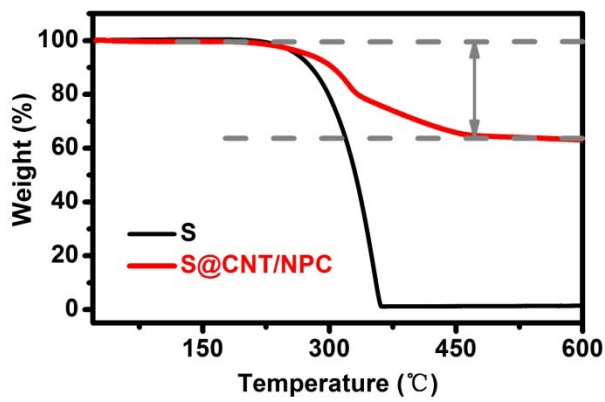


**Fig. S9.** Thermogravimetric analysis (TGA) of S@CNT/NPC composite and S under nitrogen atmosphere.

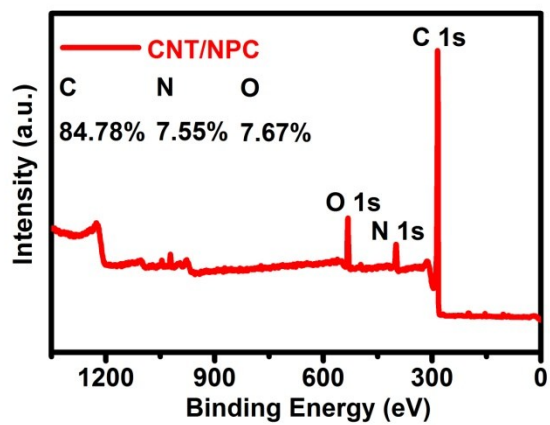


**Fig. S10.** XPS survey spectrum of CNT/NPC composite.

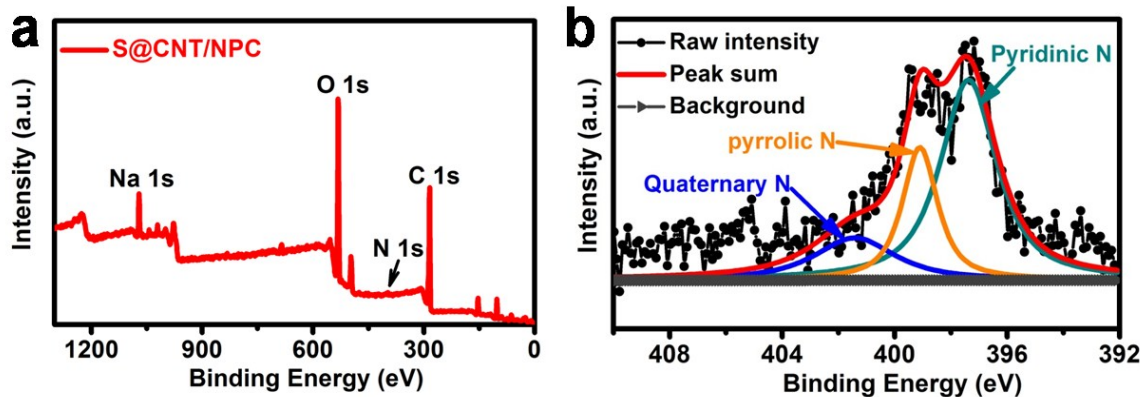


**Fig. S11.** XPS results of survey (a) and N 1s spectrum (b) of S@CNT/NPC composite after cycling.

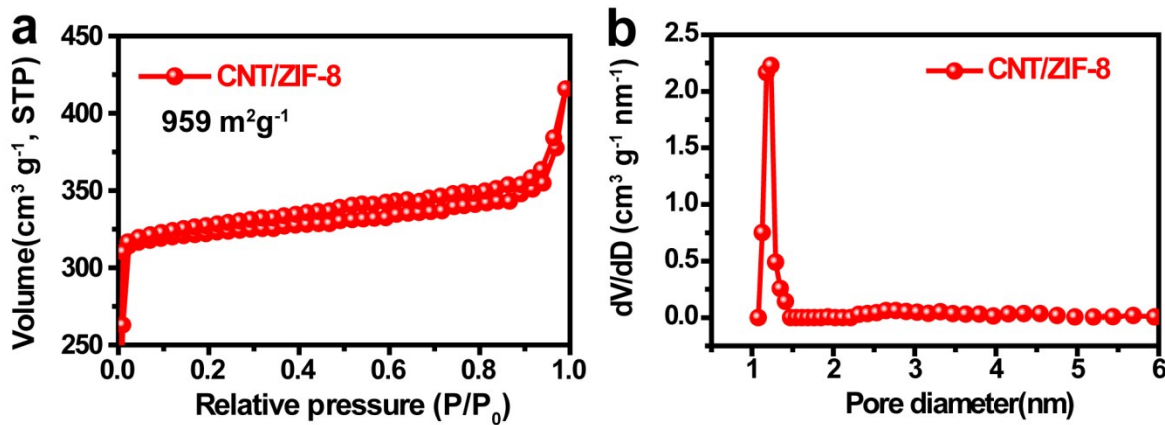


**Fig. S12.**  $\text{N}_2$  adsorption-desorption isotherms and the pore size distributions (a,b) of CNT/ZIF-8.

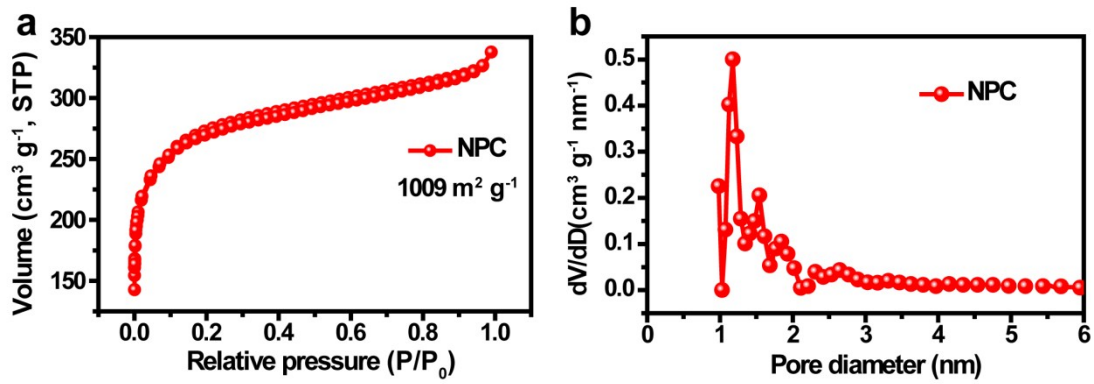


**Fig. S13.**  $\text{N}_2$  adsorption-desorption isotherms and the pore size distributions (a,b) of NPC.

Sample name	BET area ( $\text{m}^2 \text{ g}^{-1}$ )	Pore volume ( $\text{cm}^3 \text{ g}^{-1}$ )
CNT/ZIF-8	959	0.487
CNT/NPC	2480	1.011
S@CNT/NPC	20	0.101

**Fig. S14.** Comparison of BET performance between CNT/ZIF-8, CNT/NPC and S@CNT/NPC composite.

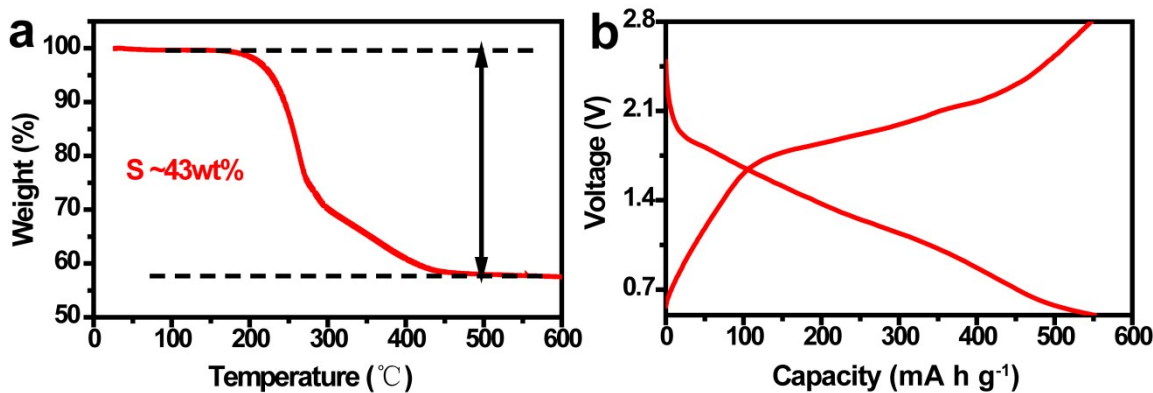


**Fig. S15.** (a) Thermogravimetric analysis (TGA) and (b) Discharge–charge curves at 0.5C of S@CNT/NPC composite electrode with 43% sulfur.

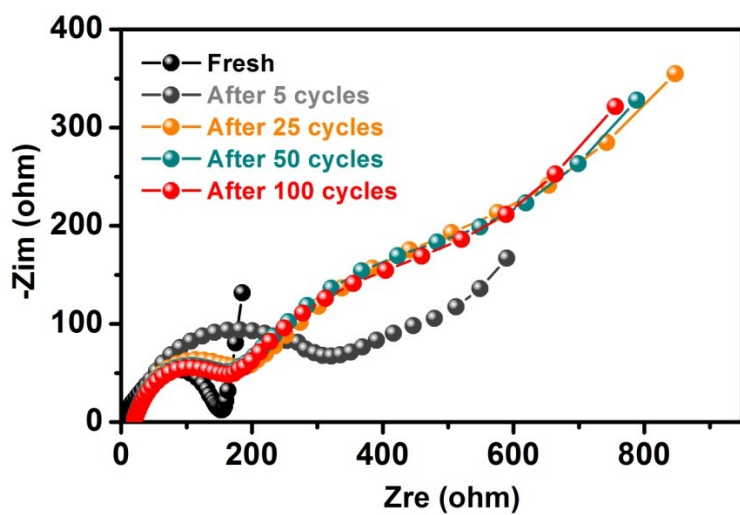


**Fig. S16.** Nyquist plots of the S@CNT/NPC composite electrodes before and after cycling.

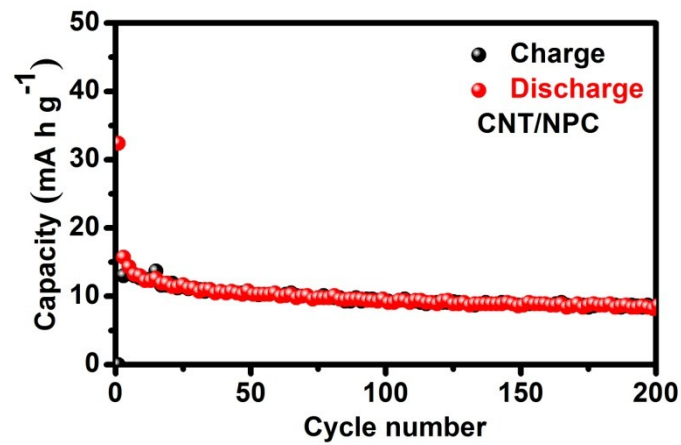


**Fig. S17.** Discharge-charge cycling performance of CNT/NPC composite electrode at 0.5C.

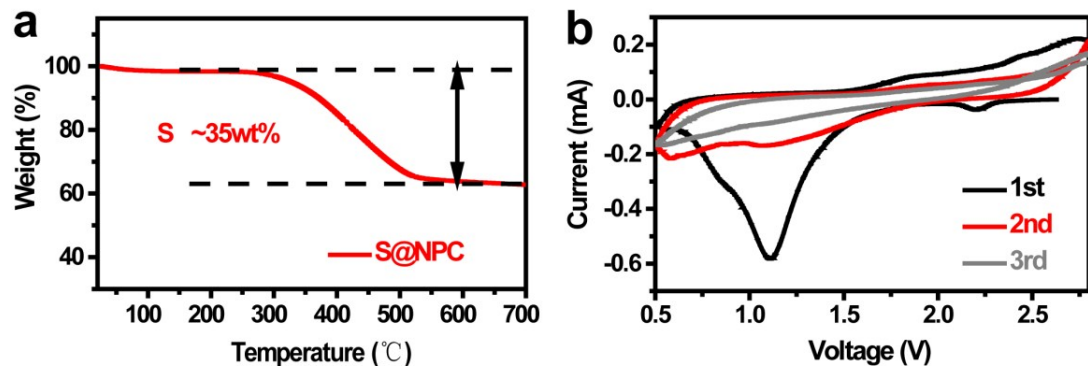


**Fig. S18.** TGA curve of the S@NPC composite under  $\text{N}_2$  atmosphere (a), CV curves of the S@NPC composite (b).

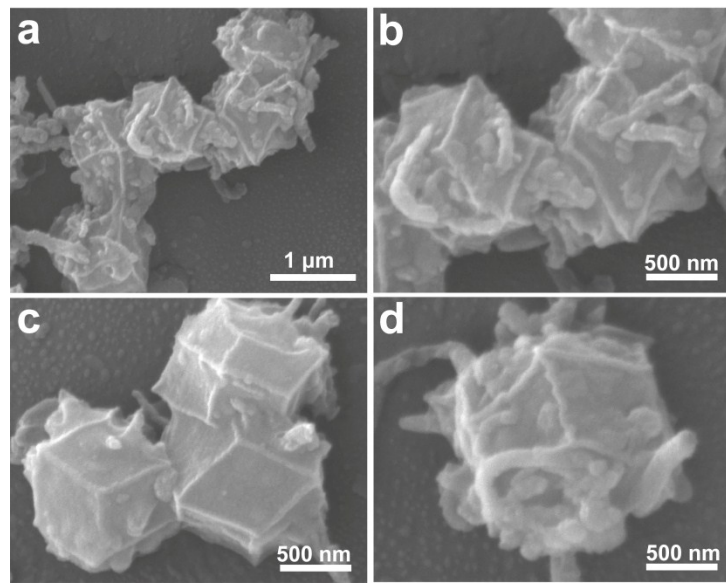


**Fig. S19.** FESEM images of S@CNT/NPC after cycles.

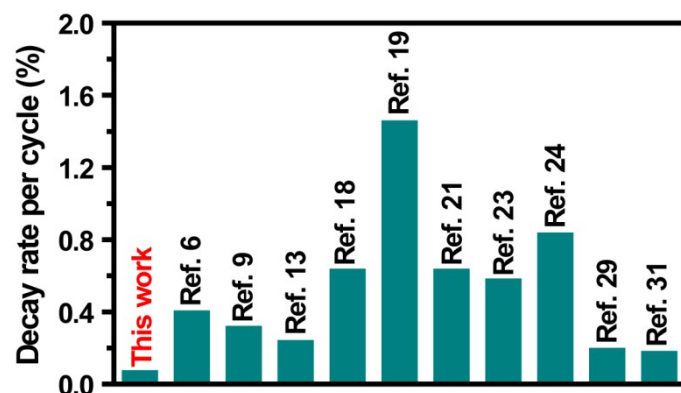


**Fig. S20.** Comparison of decay rate per cycle for S@CNT/NPC composite with references.